Supporting Information

Junker and Rief 10.1073/pnas.0904654106

SI Text

Cantilever Calibration. Calibration of cantilevers was done in solution employing the equipartition theorem (1, 2). As a control of the force calibration, unfolding forces of domain 4 of the filamin handles were recorded for all measured traces, allowing subsequent normalization of CaM forces according to the mean force of filamin 4 unfolding. Filamin domain 4 is an ideal control domain, as it is the only filamin domain in our protein construct that exhibits an unfolding intermediate, which simplifies distinguishing this domain from the other filamin domains (3).

Data Acquisition Protocol. Before data acquisition, the cantilever tip is repeatedly brought into contact with the surface by a succession of rapid approach-retract pulling cycles to mount a protein between the tip and the surface. As soon as a protein attachment to the cantilever tip has been established, the cantilever is pulled away from the surface at a low pulling velocity (e.g., 1 nm/s) to record CaM equilibrium fluctuations (Fig. S4, step 1). After forces have become so high that no transitions can be observed any more, the pulling velocity is increased to 500 nm/s, allowing observation of filamin unfolding events (Fig. S4, step 2). After unfolding of the filamin domains, the protein detaches from the tip at forces typically ≈100–500 pN. Subsequently, the cantilever is approached toward the surface again. The zero-force signal is determined by recording the force at a certain distance from the surface for 2s (Fig. S4, step 3). Afterward, the zero-extension position is determined by approaching the cantilever until it touches the surface (Fig. S4, step 4). In the end, the cantilever is moved back to the initial position.

A clear fingerprint of the filamin unfolding events was used as a criterion for a correct single-molecule attachment. Furthermore, only data that showed no unspecific surface interaction at low extension was included in the analysis. Measurements with each protein construct were performed at least twice with different cantilevers and independent sample preparations to assure reproducibility. We have measured >100 traces for the CaM-skMLCK and the CaM-CaMKK protein construct under different conditions. For each of the other protein constructs shown in the article (single domain constructs and truncated target peptides), more than 40 curves were recorded.

Monte Carlo Simulations. To gain access to parameters such as folding/unfolding rates and potential widths, Monte Carlo simulations including exact experimental conditions were performed (4). In such a simulation, we stretch a virtual polypeptide of contour length L at a certain pulling velocity, starting at zero extension. In every time step, the extension d is increased, and the force acting on the polypeptide chain at the current extension is calculated by means of the WLC interpolation formula $F(d) = (k_BT/p)\cdot[d/L + 0.25\cdot(1 - d/L)^{-2} - 0.25]$ (5). To simulate the conformational kinetics, an exponential force dependence of the unfolding rate is included in the calculation (6). For refolding, our extrapolation to zero-force conditions includes a nonexponential force dependence (7). A typical sample trace of a Monte Carlo simulation is shown in Fig. S3.

We performed single-molecule unfolding experiments of CaM-skMLCK and CaM-CaMKK at nonequilibrium conditions (i.e., at high pulling speeds) to determine k_{off} and $\Delta x_{N\text{-}TS}$ for peptide unbinding (see Fig. 5 *A* and *C*). The increase in force at higher velocities depends on the potential width for unfolding $\Delta x_{N\text{-}TS}$ (8, 9). Monte Carlo simulations could reproduce the experimental data best with the potential widths for unfolding and the zero-force unbinding rates $k_{off}(F = 0)$ shown in Fig. 5 *B* and *D*. The values we find for $\Delta x_{N\text{-}TS}$ are in the same range as the potential widths for unfolding of DomN and DomC (10). k_{off} (F = 0) and $\Delta x_{N\text{-}TS}$ for skMLCK and CaMKK can now be used to simulate the equilibrium traces at a pulling velocity of, for example, 1 nm/s. For the potential width for folding $\Delta x_{TS\text{-}U}$, we used the actual length of the unfolded protein at the applied force, from which we subtracted the length of the folded protein and the distance to the transition state. The additional folding barrier under force is calculated as the free energy $E_{fold}(F, \Delta L, L)$ needed to contract the unfolded protein of length ΔL to the length of its transition state while it is attached to the AFM cantilever tip via a polypeptide spacer of length L (11). We then adapted the folding rate to match the experimental traces. As a control, we compared the free energy of binding as calculated from the binding and unbinding rate, $\Delta G = \ln(k_{off}/k_{on})$, to the binding free energy as estimated from the area enclosed by the upper and the middle level in the traces.

Calculation of Contour Length Increases. Contour length increases (ΔL) were determined by fitting WLC curves calculated using the interpolation formula by Bustamante et al. (5) with a fixed persistence length of 0.5 nm. Contour length increases were used to calculate the number of amino acids *n* involved in an unfolding event via $\Delta L = n\cdot d_{aa} - d_{folded}(I) + d_{folded}(II)$. Here, $d_{folded}(I)$ and $d_{folded}(II)$ denote the end-to-end distances of the folded structure before and after the unfolding event, respectively, as determined from the crystal structure [2BBM (12) and 1CKK (13)]. d_{aa} is the contour length increase per amino acid, which has been determined to be 0.365 ± 0.002 nm for our instrument at a persistence length of 0.5 nm (14). An analysis of the increases in contour length that follow the unfolding events allows us to obtain more detailed insights into unbinding and unfolding on a structural level. However, slight deviations of ≈1–2 nm from the expected values might occur because of a possible deformation of CaM under force. Moreover, the domain boundaries of CaM are not precisely defined.

Fitting WLC curves to the traces obtained for CaM-skMLCK at 100 μM mastoparan and v_{pull} = 10 nm/s, we find a value of ΔL_I = 16.5 ± 1.4 nm for the first unfolding event, which is larger than the expected value of $\Delta L_{skMLCK} = 0.365\ nm\cdot(n_{skMLCK} + n_{Spacer}) - d_{CaM\text{-}skMLCK} + d_{CaM} = 0.365\ nm\cdot(23 + 4) - 2.4\ nm + 1.7\ nm = 9.2\ nm$ for unbinding of skMLCK (Fig. S1 and Table S1). (Here we assumed that the three C-terminal amino acid residues of skMLCK, which are clearly outside the binding pocket in the crystal structure, are not bound and, hence, do not contribute to the increase in contour length.) This suggests a part of the central interdomain linker (≈15 aa residues) unfolds together with the target peptide leading to $\Delta L_{skMLCK} = 0.365\ nm\cdot(n_{skMLCK} + n_{Spacer} + n_{Linker}) - d_{CaM\text{-}skMLCK} + d_{DomN} + d_{DomC} = 0.365\ nm\cdot(23 + 4 + 15) - 2.4\ nm + 2.1\ nm + 1.4\ nm = 16.4\ nm$. The two subsequent unfolding events lead to an overall increase in contour length of $\Delta L_{II} + \Delta L_{III}$ = 46.7 ± 1.3 nm, which is close to the expected value of $\Delta L_{CaM} = 0.365\ nm\cdot 133 - 2.1\ nm - 1.4\ nm = 45.4\ nm$ (Fig. S1 and Table S1). The observation that the central linker unfolds upon target peptide unbinding shows that skMLCK holds together the two domains of CaM, thereby screening the mechanically unstable interdomain linker from the applied force. After skMLCK unbinding, the linker is exposed to force and unfolds immediately.

For CaM-CaMKK, we obtain a value of $\Delta L_I + \Delta L_{III}$ = 24.0 ±

1.3 nm for the sum of both peptide unbinding transitions, which is significantly larger than the expected value of ΔL_{CaMKK} = 0.365 nm · (n_{CaMKK} + n_{Spacer} + n_{Linker}) − $d_{CaM\text{-}CaMKK}$ + d_{DomN} + d_{DomC} = 0.365 nm · (26 + 8 + 15) − 1.2 nm + 1.9 nm + 1.5 nm = 20.1 nm, while the sum of both CaM unfolding events, ΔL_{II} + ΔL_{IV} = 40.5 ± 1.4 nm, is smaller than the expectation value ΔL_{CaM} = 0.365 nm · 133 − 1.9 nm − 1.5 nm = 45.1 nm (Fig. S1 and Table S1). Since the lower contour length increases upon CaM unfolding can be attributed exclusively to DomN with ΔL_{II} = 17.7 ± 1.4 nm as compared to an expected value of L_{DomN} = 0.365 nm · 70 − 1.9 nm = 23.7 nm, we assume a part of CaMKK N rebinds to DomC after unfolding of DomN, thereby shortening the effective increase in contour length ΔL_{II} and increasing ΔL_I + ΔL_{III} by ≈5 nm. The overall increase in contour length of the four transitions of CaM-CaMKK (ΔL_I + ΔL_{II} + ΔL_{III} + ΔL_{IV} = 64.5 nm) is in good agreement with the expected value of $\Delta L_{CaM\text{-}CaMKK}$ = 0.365 nm · (n_{CaM} + n_{CaMKK} + n_{Spacer}) − $d_{Cam\text{-}CaMKK}$ = 0.365 nm · (148 + 26 + 8) − 1.9 nm = 65.2 nm, suggesting a high precision of contour length measurements.

Free Energy of Ligand Binding. In thermodynamic equilibrium with respect to ligand binding/unbinding, the free energy of interaction for *n* ligands binding to a protein can be calculated as ΔG_b = $k_BT{\cdot}\ln\Sigma$, where $\Sigma = 1+c/K_1+c^2/K_2+..+c^n/K_n$ is the binding polynomial (K_i, *i*th phenomenological dissociation constant; c, ligand concentration) (15). If only one ligand binds to the protein (e.g., peptide binding to one CaM domain), the formula reduces to $\Delta G_b = k_BT{\cdot}\ln(1+c/K)$, in the case of two ligands per protein (e.g., Ca^{2+} binding to one CaM domain), we get $\Delta G_b = k_BT{\cdot}\ln(1+c/K_1+c^2/K_2)$. In the context of folding, where we measure the free energy difference between the folded and the unfolded state, we have to take into account the dissociation constants of the folded state K_i^N and the unfolded state K_i^U to calculate the increase in free energy difference upon ligand binding (16, 17). We then get $\Delta G_b = k_BT{\cdot}[\ln(1+c/K^N{}_1+c^2/K^N{}_2) - \ln(1+c/K^U{}_1+c^2/K^U{}_2)]$ in the case of Ca^{2+}. Therefore, even at concentrations well above the dissociation constant of the native state, the free energy of ligand binding increases logarithmically with the ligand concentration until the dissociation constant of the unfolded state is reached. Therefore, the measurements shown here were performed at a relatively high calcium concentration of 10 mM to increase the stability of calmodulin, which increases the signal-to-noise ratio and simplifies data analysis.

1. Butt HJ, Jaschke M (1995) Calculation of thermal noise in atomic-force microscopy. *Nanotechnology* 6:1–7.
2. Florin EL, et al. (1995) Sensing specific molecular-interactions with the atomic-force microscope. *Biosens Bioelectron* 10:895–901.
3. Schwaiger I, Kardinal A, Schleicher M, Noegel AA, Rief M (2004) A mechanical unfolding intermediate in an actin-crosslinking protein. *Nat Struct Mol Biol* 11:81–85.
4. Rief M, Fernandez JM, Gaub HE (1998) Elastically coupled two-level-systems as a model for biopolymer extensibility. *Phys Rev Lett* 81:4764–4767.
5. Bustamante C, Marko JF, Siggia ED, Smith S (1994) Entropic elasticity of lambda-phage DNA. *Science* 265:1599–1600.
6. Bell GI (1978) Models for the specific adhesion of cells to cells. *Science* 200:618–627.
7. Schlierf M, Rief M (2009) Surprising simplicity in the single-molecule folding mechanics of proteins. *Angew Chem Int Ed Engl* 48:820–822.
8. Evans E, Ritchie K (1997) Dynamic strength of molecular adhesion bonds. *Biophys J* 72:1541–1555.
9. Rief M, Gautel M, Oesterhelt F, Fernandez JM, Gaub HE (1997) Reversible unfolding of individual titin immunoglobulin domains by AFM. *Science* 276:1109–1112.
10. Junker JP, Ziegler F, Rief M (2009) Ligand-dependent equilibrium fluctuations of single calmodulin molecules. *Science* 323:633–637.
11. Schlierf M, Berkemeier F, Rief M (2007) Direct observation of active protein folding using lock-in force spectroscopy. *Biophys J* 93:3989–3998.
12. Ikura M, et al. (1992) Solution structure of a calmodulin-target peptide complex by multidimensional NMR. *Science* 256:632–638.
13. Osawa M, et al. (1999) A novel target recognition revealed by calmodulin in complex with Ca2+-calmodulin-dependent kinase kinase. *Nat Struct Biol* 6:819–824.
14. Dietz H, Rief M (2004) Exploring the energy landscape of GFP by single-molecule mechanical experiments. *Proc Natl Acad Sci USA* 101:16192–16197.
15. Schellman JA (1975) Macromolecular binding. *Biopolymers* 14:999–1018.
16. Masino L, Martin SR, Bayley PM (2000) Ligand binding and thermodynamic stability of a multidomain protein, calmodulin. *Protein Sci* 9:1519–1529.
17. Kellis JT, Jr, Todd RJ, Arnold FH (1991) Protein stabilization by engineered metal chelation. *Biotechnology (N Y)* 9:994–995.

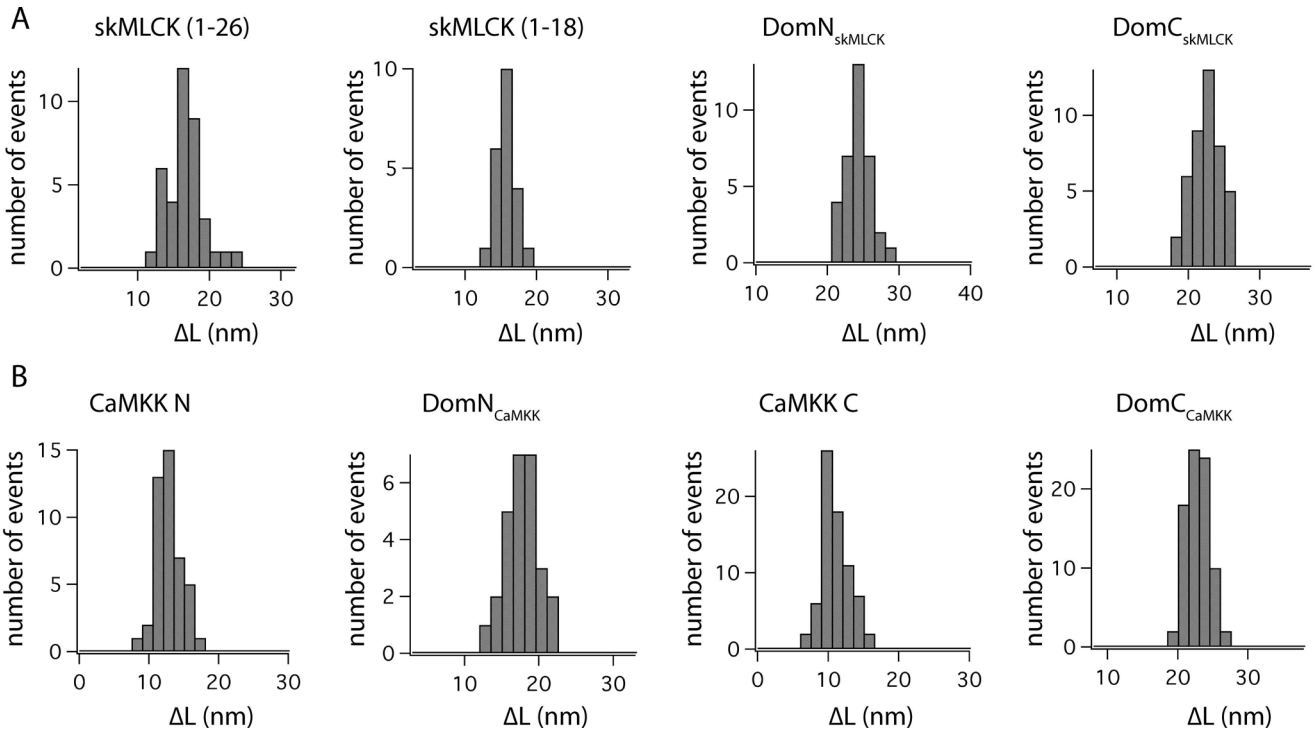

Fig. S1. Contour length histograms of the various unfolding transitions of CaM-skMLCK (*a*) and CaM-CaMKK (*b*). Values for ΔL were obtained by fitting WLC curves to force vs. extension traces that were recorded at v_{pull} = 10 nm/s and [mastoparan] = 100 μM.

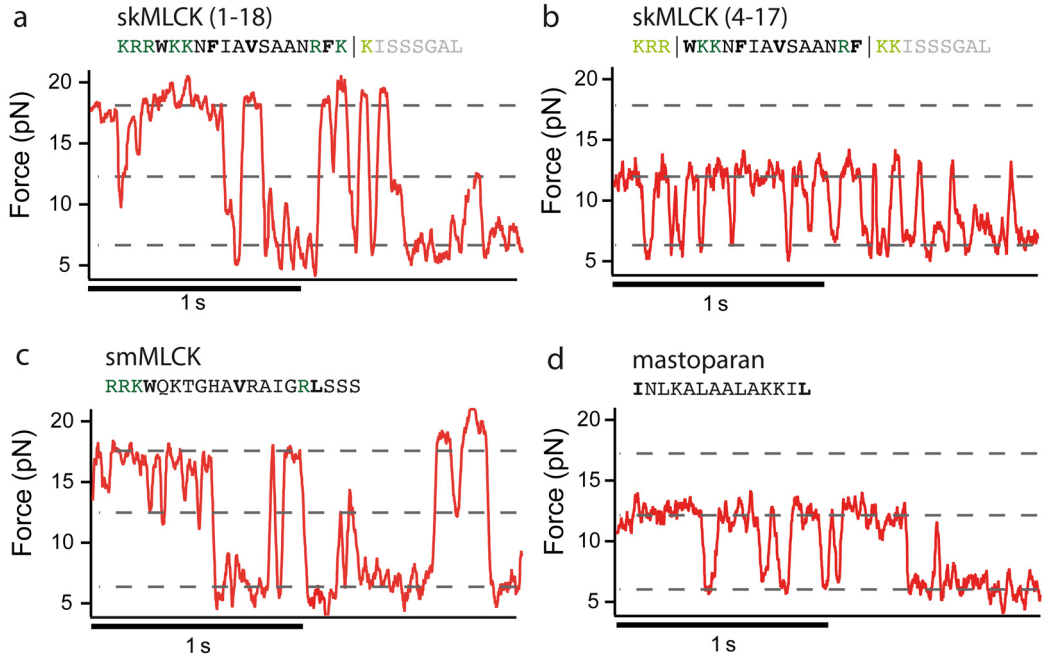

Fig. S2. Time traces of the transition region of DomN. (*a*) CaM-skMLCK (1–18); (*b*) CaM-skMLCK (4–17); (*c*) CaM-smMLCK; (*d*) CaM-mastoparan. While an intermediate state can be observed for CaM-skMLCK (1–18) and CaM-smMLCK (dashed middle level), no corresponding state exists for CaM-skMLCK (4–17) and CaM-mastoparan, suggesting no sufficiently stable bond is formed between CaM and the latter two peptides. In the amino acid sequence of the target peptides, hydrophobic anchor residues are shown in bold font. Amino acid residues that have been removed are colored in gray and light green.

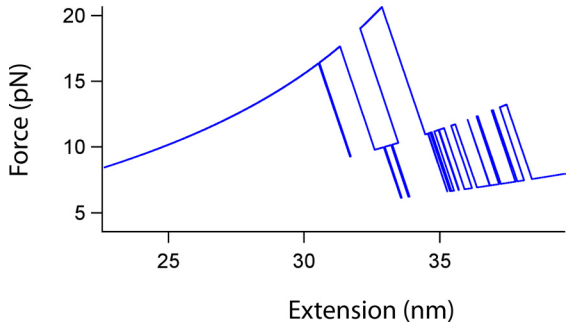

Fig. S3. Sample trace of Monte Carlo simulation showing transitions between 3 states (folded, peptide-bound; folded, peptide-unbound; unfolded).

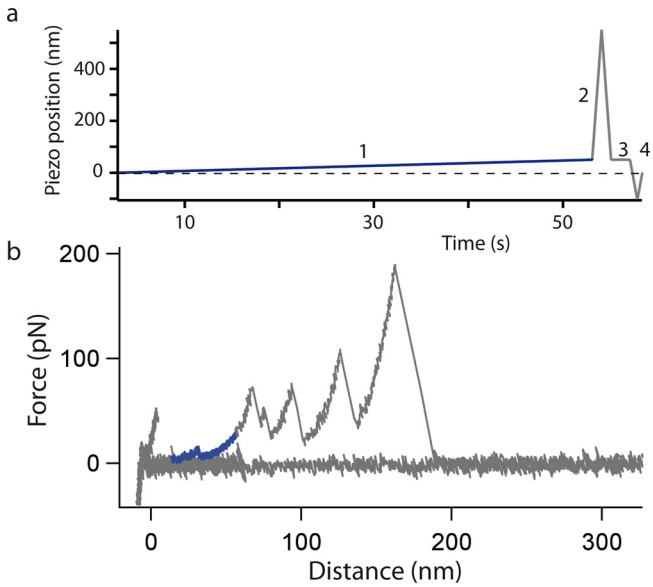

Fig. S4. Sketch of the data acquisition protocol (*a*) and corresponding force vs. extension trace (*b*). In the beginning, the cantilever tip is repeatedly brought into contact with the surface to mount a protein between the tip and the surface. Now, the cantilever is pulled away from the surface at a low pulling velocity (here, 1 nm/s) to record CaM equilibrium fluctuations (1). Finally, forces become so high that no transitions can be observed any more. Then, the pulling velocity is increased to 500 nm/s, so that also the filamin domains are unfolded, which serves as a control for correct attachment of a single protein chain (2). After unfolding of the filamin domains, the protein detaches from the tip at forces typically ~100–500 pN. Subsequently, the cantilever is approached toward the surface again. The zero-force signal is determined by recording the force at a certain distance from the surface for 2s (3). Afterward, the zero-extension position is determined by approaching the cantilever until it touches the surface (4). In the end, the cantilever is moved back to the initial position.

Table S1. Contour length increases of CaM-skMLCK and CaM-CaMKK protein constructs

Protein constructs	ΔL skMLCK/CaM_{KK}
skMLCK(1–26)	16.5 ± 1.4 nm
skMLCK(1–18)	15.5 ± 1.3 nm
$DomN_{skMLCK}$	24.3 ± 1.3 nm
$DomC_{skMLCK}$	22.4 ± 1.3 nm
CKK N	12.9 ± 1.3 nm
$DomN_{CaMKK}$	17.7 ± 1.4 nm
CKK C	11.1 ± 1.2 nm
$DomC_{CaMKK}$	22.8 ± 1.2 nm

Errors are calculated as SEM + 1.0 nm systematic error (errors in zero-extension and zero-force determination, drift in x and y direction, errors from fitting in different force regimes)

Table S2. Contour length increases and mean unbinding forces of DomC-CaMKK(1–26) and DomC-CaMKK(9–26)

CaMKK truncation	ΔL CaMKK	ΔL DomC	F
CaMKK(1–26)	11.5 ± 1.4 nm	23.1 ± 1.4 nm	15.1 ± 0.6 pN
CaMKK(9–26)	11.2 ± 1.4 nm	22.7 ± 1.3 nm	15.3 ± 0.5 pN

Contour length increases and mean unbinding forces of truncated CaMKK are indistinguishable from the full-length peptide.